Why all crystals need not be bcc: Symmetry breaking at the liquid-solid transition revisited

B. Groh and B. Mulder
FOM Institute for Atomic and Molecular Physics, Kruislaan 407, 1098 SJ Amsterdam, The Netherlands
(Received 30 October 1998)

Alexander and McTague [Phys.Rev. Lett. **41**, 702 (1978)] argued that if there is a spinodal point associated with the liquid-solid transition in a fluid of spherically symmetric particles, the bcc phase will be uniquely favored as the only accessible symmetry breaking structure that forms a regular three-dimensional lattice. By reconsidering their analysis in the framework of density-functional theory, we show that at a liquid-solid spinodal in fact many other solid stuctures also are simultaneously accessible, among them the fcc structure. Nevertheless, the bcc structure is still shown to be special, as, independent of the details of the interaction, the free energy of the unstable bcc phase close to the spinodal is always lower than that of the other solidlike structures. We illustrate our general results by explicit calculations on a toy model, the ''Onsager solid.'' This simple model also indicates that the ultimately stable crystal phase, which, as usual for sufficiently steep repulsive forces, turns out to be fcc, is dictated by properties of the free energy that cannot be obtained perturbatively starting from the spinodal point. [S1063-651X(99)00905-8]

PACS number(s): 64.70.Dv, 61.50.Ah, 64.60.−i

I. INTRODUCTION

Landau theory [2,3] is a powerful tool for the analysis of symmetry-related aspects of phase transitions. In a seminal paper [1], Alexander and McTague applied it to the freezing transition of monatomic fluids of spherically symmetric particles. Their most striking result was that the bcc phase should be uniquely favored independent of the interaction details. However, a number of real metals and the rare gases as well as many model systems, such as the hard sphere and the Lennard-Jones fluid, actually freeze into an fcc solid phase. The latter is also predicted by the elaborate density-functional theories that have been developed in the past decades [4,5].

Still the bcc structure seems to play an important role in nucleation processes. A large number of computer simulation studies have examined the possibility of bcc nuclei in the supercooled Lennard-Jones liquid, with controversial results. The most recent and most sophisticated work, by ten Wolde *et al.* [6,7], reported small bcc nuclei that attain an fcc core upon growing while the surface remains bcc-like. This was confirmed within a density-functional theory by Shen and Oxtoby [8], who furthermore showed that the equilibrium solid-liquid interface locally has bcc character, too. Thus the bcc structure seems to be closer to the liquid than the fcc in a not yet fully understood sense.

In the present work we readdress this problem from a somewhat different perspective using a combination of density-functional theory and the Landau approach. In principle, a Landau expansion can be derived from any given approximation to the density functional by considering small solidlike perturbations of the liquid state. More insight can be gained when one looks at solutions of the Euler-Lagrange equation that follows from the density-functional theory, which represent the stable and metastable states as well as the saddle points in the infinite dimensional space of density profiles. We will present a generic picture of the typical global behavior of these solutions for bcc and fcc structures. In both cases a solution branch bifurcates from the liquid state at the stability limit of the liquid, i.e., the liquid-solid spinodal, which turns out to be the same thermodynamic point for both bcc and fcc solids. We determine the asymptotic form of the solutions along these branches by bifurcation analysis. Using arguments closely related to those of Alexander and McTague, a fundamentally different behavior is obtained for bcc and fcc. However, with the help of the global picture one realizes that these findings only apply to the unstable solution branches near the spinodal point, while no similarly general statement can be made about the stable branches that are typically far off from the liquid in a ''solid order parameter space'' and cannot be described by one or a small number of density Fourier coefficients. From this perspective it is no surprise that in many cases the fcc solid is thermodynamically stable in spite of the preference for bcc at low crystallinity.

II. BIFURCATION ANALYSIS OF DENSITY-FUNCTIONAL THEORIES

The free-energy functional for a one-component fluid of spherical particles has the general form

$$F[\{\rho(\mathbf{r})\}]=k_BT\int d^3\,\rho(\mathbf{r})[\ln\rho(\mathbf{r})\lambda^3-1]+F_{\mathrm{ex}}[\{\rho(\mathbf{r})\}] \tag{1}$$

with the thermal wavelength λ. The first term represents the ideal gas entropy while the excess free energy F_{ex} depends on the details of the particle interactions and is not known exactly except in trivial cases. However, a large number of approximative expressions for F_{ex} are available for simple models, especially for the hard sphere fluid [4,5]. These are capable of predicting the location of the freezing transition and the solid structure with satisfactory accuracy.

In order to obtain the equilibrium density profile $\rho(\mathbf{r})$ for a given bulk density ρ_b, the free-energy functional is mini-

mized under the constraint $\int d^3r\rho(\mathbf{r})=V\rho_b$, i.e., using a Lagrange multiplier μ, which yields the Euler Lagrange equation

$$\ln\rho(\mathbf{r})\lambda^3-c^{(1)}(\{\rho(\mathbf{r})\},\mathbf{r})-\beta\mu=0. \tag{2}$$

The direct correlation functions $c^{(n)}$ are defined as functional derivatives of the excess functional:

$$c^{(n)}(\{\rho(\mathbf{r})\},\mathbf{r}_1,\ldots,\mathbf{r}_n)=-\beta\frac{\delta^n F_{\mathrm{ex}}[\{\rho(\mathbf{r})\}]}{\delta\rho(\mathbf{r}_1)\delta\rho(\mathbf{r}_2)\cdots\delta\rho(\mathbf{r}_n)}. \tag{3}$$

Elimination of the Lagrange multiplier from Eq. (2) using the normalization condition yields

$$\ln\rho(\mathbf{r})-\frac{1}{V}\int d^3r'\ln\rho(\mathbf{r}')-c^{(1)}(\{\rho(\mathbf{r})\},\mathbf{r}) +\frac{1}{V}\int d^3r'c^{(1)}(\{\rho(\mathbf{r})\},\mathbf{r}')=0. \tag{4}$$

We now employ a Fourier representation of the density

$$\rho(\mathbf{r})=\rho_b\left(1+\sum_{\mathbf{q}}\eta(q)e^{i\mathbf{q}\cdot\mathbf{r}}\right) \tag{5}$$

with a possibly infinite but discrete set of wave vectors $\mathbf{q}$ and $\eta(0)=0$ to ensure correct normalization. We require the origin $\mathbf{r}=\mathbf{0}$ to be a symmetry point of the lattice so that $\eta(\mathbf{q})$ must be invariant under all point symmetries. Therefore, it depends only on the absolute value of $\mathbf{q}$. After insertion of Eq. (5) into Eq. (2) or Eq. (4), Fourier transformation, and expansion of the logarithm, one obtains for $\mathbf{q}\neq\mathbf{0}$

$$\sum_{n=1}^{\infty}\frac{(-1)^{n+1}}{n}\sum_{\mathbf{q}_1}\cdots\sum_{\mathbf{q}_n}\eta(q_1)\cdots\eta(q_n)\delta\left(\mathbf{q}-\sum_i\mathbf{q}_i\right) -\frac{1}{V}\int d^3re^{-i\mathbf{q}\cdot\mathbf{r}}c^{(1)}(\{\rho(\mathbf{r})\},\mathbf{r})=0. \tag{6}$$

The homogeneous density $\rho(\mathbf{r})=\rho_b$ always solves Eq. (6) because $c^{(1)}(\rho_b,\mathbf{r})$ is a constant, but one expects that beyond a critical bulk density ρ_c it no longer corresponds to a local minimum of the density functional but rather to a saddle point.

By a bifurcation analysis of Eq. (6) we shall determine the stability limit ρ_c of the liquid solution as well as the character of the bifurcating solutions that become stable above ρ_c. To this end we expand the bulk density ρ_b and the Fourier components $\eta(q)$ with respect to a small dimensionless parameter ϵ:

$$\rho_b=\rho_c+\epsilon\rho_1+\epsilon^2\rho_2+\cdots, \tag{7}$$

$$\eta(q)=\epsilon\eta_1(q)+\epsilon^2\eta_2(q)+\cdots, \tag{8}$$

which is inserted into Eq. (6) and then sorted according to powers of ϵ yielding a hierarchy of bifurcation equations of which the first three are

$$\eta_1(q)[1-\rho_c\tilde{c}^{(2)}(\rho_c,q)]=0, \tag{9}$$

$$-\eta_1(q)\rho_1\tilde{c}^{(2)}(q)+\eta_2(q)[1-\tilde{c}^{(2)}(q)]-\rho_c\rho_1\eta_1(q) \times\tilde{c}^{(3)}(q,0)-\frac{1}{2}\sum_{\mathbf{q}_1,\mathbf{q}_2}\delta(\mathbf{q}-\mathbf{q}_1-\mathbf{q}_2)\eta_1(q_1)\eta_1(q_2) \times[1+\rho_c^2\tilde{c}^{(3)}(\mathbf{q}_1,\mathbf{q}_2)]=0, \tag{10}$$

and

$$\eta_3(q)-\tilde{c}^{(2)}(q)[\rho_2\eta_1(q)+\rho_1\eta_2(q)+\rho_c\eta_3(q)]-\tilde{c}^{(3)}(q,0)[\rho_1^2\eta_1(q)+\rho_1\rho_2\eta_2(q)+\rho_2\rho_c\eta_1(q)] -\sum_{\mathbf{q}_1,\mathbf{q}_2}\delta(\mathbf{q}-\mathbf{q}_1-\mathbf{q}_2)\left\{\eta_1(q_1)\eta_1(q_2)\left[\tilde{\rho}_c\rho_1c^{(3)}(\mathbf{q}_1,\mathbf{q}_2)+\frac{1}{2}\rho_1\rho_c^2\tilde{c}^{(4)}(\mathbf{q}_1,\mathbf{q}_2,0)\right]+\eta_1(q_1)\eta_2(q_2)[1+\rho_c^2\tilde{c}^{(3)}(\mathbf{q}_1,\mathbf{q}_2)]\right\} -\frac{1}{2}\tilde{c}^{(4)}(q,0,0)\rho_1^2\rho_c\eta_1(q)-\frac{1}{6}\sum_{\mathbf{q}_1,\mathbf{q}_2,\mathbf{q}_3}\delta(\mathbf{q}-\mathbf{q}_1-\mathbf{q}_2-\mathbf{q}_3)\eta_1(q_1)\eta_1(q_2)\eta_1(q_3)[\rho_c^3\tilde{c}^{(4)}(\mathbf{q}_1,\mathbf{q}_2,\mathbf{q}_3)-2]=0. \tag{11}$$

Here $\tilde{c}^{(n)}(\rho,\mathbf{q}_1,\ldots,\mathbf{q}_{n-1})$ denotes the Fourier transform of the nth liquid direct correlation function:

$$\tilde{c}^{(n)}(\rho,\mathbf{q}_1,\ldots,\mathbf{q}_{n-1})=\int d^3r_1\cdots d^3r_{n-1}c^{(n)}(\rho,\mathbf{r}_1,\ldots,\mathbf{r}_n) \times e^{-i\mathbf{q}_1\cdot(\mathbf{r}_1-\mathbf{r}_n)}\cdots e^{-i\mathbf{q}_{n-1}\cdot(\mathbf{r}_{n-1}-\mathbf{r}_n)}. \tag{12}$$

When the density argument of $\tilde{c}^{(n)}$ is omitted, as in Eqs. (10) and (11), it is understood to be ρ_c.

The first bifurcation equation determines the critical (i.e., spinodal) density as the smallest solution of

$$1-\rho_c\tilde{c}^{(2)}(\rho_c,q)=0. \tag{13}$$

It occurs at the wave number q^* of the global maximum of

$\tilde{c}^{(2)}(\rho_c,q)$, which determines the wavelength and thus the lattice constant of the bifurcating solid solution. We remark that this lattice constant will in general deviate from the one that follows by the restriction of one particle per unit cell at the bulk density ρ_c. The ρ_c defined in this way is independent of the lattice structure. This means that solutions with different structures can branch off from the liquid branch at the same density. Equation (9) also shows that $\eta_1(q)=0$ for all $\mathbf{q}$ with $q\neq q^*$.

Let us now consider the second bifurcation equation for a wave vector $\mathbf{q}$ in the first shell (i.e., $|\mathbf{q}|=q^*$) for which the terms with $\eta_2(q)$ drop out due to Eq. (13). There are two fundamentally different possibilities, depending on whether the sum over $\mathbf{q}_1$ and $\mathbf{q}_2$ in Eq. (10) reduces to zero or not. The former will occur if the sum of any two wave vectors $\mathbf{q}_1$ and $\mathbf{q}_2$ of the first shell never equals another vector in this shell, i.e., if equilateral triangles cannot be formed by the vectors in the first shell. This is actually the case for most conceivable solid structures, e.g., simple cubic, where the first shell consists of the six vectors obtained from $q^*(1,0,0)$ by sign changes and permutations of the components, and also for fcc, where the eight vectors of the first shell can be generated from $q^*/\sqrt{3}\,(1,1,1)$. We recognize the above condition for the nonvanishing of the sum as Alexander and McTague's condition for the occurrence of a third-order term in the Landau free energy [1]. They found that the only possibility for a nonzero sum that is compatible with a three-dimensional periodic lattice corresponds to the bcc structure whose first shell in reciprocal space is formed by the twelve vectors generated by $q^*/\sqrt{2}\,(1,1,0)$. The thirty vectors given by the edges of a regular icosahedron also allow the formation of equilateral triangles but do not produce periodic structures. However, this case may be relevant for quasicrystals whose refraction patterns do exhibit icosahedral symmetry [9]. A third, rather unlikely possibility also mentioned by Alexander and McTague is a two-dimensional triangular lattice generated by the six vectors pointing from the center to the vertices of a regular hexagon.

The liquid state direct correlation functions $c^{(n)}$ are invariant under any $O(3)$ transformation acting simultaneously on all arguments $\mathbf{r}_1,\ldots,\mathbf{r}_n$. By choosing $\mathbf{r}_n=\mathbf{0}$ in Eq. (12) one concludes that their Fourier transforms are also invariant under $O(3)$ transformations of $\mathbf{q}_1,\ldots,\mathbf{q}_{n-1}$. As any two equilateral triangles with one corner at the origin can be transformed into each other by a rotation, all terms in the sum of Eq. (10) are equal. For the bcc lattice there are four such terms. The magnitude of ρ_1 is actually irrelevant since it just sets the ϵ scale. Therefore we can set $\rho_1=\rho_c$ and obtain

$$\eta_1(q^*)=-\frac{1+\rho_c^2\tilde{c}^{(3)}(q^*,0)}{2[1+\rho_c^2\tilde{c}^{(3)}(\mathbf{q}_1,\mathbf{q}_2)]}, \tag{14}$$

where $\mathbf{q}_1$ and $\mathbf{q}_2$ are any two vectors of the first shell such that $|\mathbf{q}_1|=|\mathbf{q}_2|=|\mathbf{q}_1+\mathbf{q}_2|$.

However, solutions of other type, e.g., fcc, may also exist when $\rho_1=0$. In order to construct these solutions to lowest order in ϵ one must take into account vectors of the second shells, i.e., those that can be reached by the summation of two first shell vectors. For fcc three different second shells contribute, which are generated by permutations and sign changes of the vectors $\mathbf{q}_{200}=q^*/\sqrt{3}\,(2,0,0)$, $\mathbf{q}_{220}=q^*/\sqrt{3}\,(2,2,0)$, and $\mathbf{q}_{222}=q^*/\sqrt{3}\,(2,2,2)$. Equation (11) evaluated for q^* and Eq. (10) evaluated for $\mathbf{q}$ in one of the second shells form a coupled sytem of equations which determines $\eta_1(q^*)$, $\eta_2(q_{200})$, $\eta_2(q_{200})$, and $\eta_2(q_{200})$. The number of possibilities to write a given second shell vector as a sum of two first shell vectors is 4, 2, and 1 for the shells (200), (220), and (222), respectively, and $\Sigma_{\mathbf{q}_1,\mathbf{q}_2}\delta(\mathbf{q}-\mathbf{q}_1-\mathbf{q}_2)$ with $q=q_1=q^*$ gives 3, 3, and 1 for the three cases of second shell vectors $\mathbf{q}_2$. Using $\rho_2=\pm\rho_c$ to allow for solutions above and below ρ_c, one gets

$$\eta_2(q_{200})[1-\rho_c\tilde{c}^{(2)}(q_{200})]-2\eta_1^2(q^*)[1+\rho_c^2\tilde{c}^{(3)}(\mathbf{q}_1,\mathbf{q}_{200})]=0, \tag{15}$$

$$\eta_2(q_{220})[1-\rho_c\tilde{c}^{(2)}(q_{220})]-\eta_1^2(q^*)[1+\rho_c^2\tilde{c}^{(3)}(\mathbf{q}_1,\mathbf{q}_{220})]=0 \tag{16}$$

$$\eta_2(q_{222})[1-\rho_c\tilde{c}^{(2)}(q_{222})]-\frac{1}{2}\eta_1^2(q^*)[1+\rho_c^2\tilde{c}^{(3)}(\mathbf{q}_1,\mathbf{q}_{222})]=0, \tag{17}$$

and

$$\begin{aligned}&\mp\rho_c\tilde{c}^{(2)}(q^*)\mp\rho_c^2\tilde{c}^{(3)}(q^*,0)-3\eta_2(q_{200})\\&\quad\times[\rho_c^2\tilde{c}^{(3)}(\mathbf{q}_1,\mathbf{q}_{200})+1]\\&-3\eta_2(q_{220})[\rho_c^2\tilde{c}^{(3)}(\mathbf{q}_1,\mathbf{q}_{220})+1]-\eta_2(q_{222})\\&\quad\times[\rho_c^2\tilde{c}^{(3)}(\mathbf{q}_1,\mathbf{q}_{222})+1]-\frac{1}{6}\eta_1^2(q^*)\\&\quad\times\sum_{\mathbf{q}_1,\mathbf{q}_2,\mathbf{q}_3}\delta(\mathbf{q}-\mathbf{q}_1-\mathbf{q}_2-\mathbf{q}_3)[2\rho_c^3\tilde{c}^{(4)}(\mathbf{q}_1,\mathbf{q}_2,\mathbf{q}_3)-1]\\&=0,\end{aligned} \tag{18}$$

where the arguments of $\tilde{c}^{(3)}$ in Eqs. (15)–(18) are chosen so that $|\mathbf{q}_1|=|\mathbf{q}_1+\mathbf{q}_{200}|=|\mathbf{q}_1+\mathbf{q}_{220}|=|\mathbf{q}_1+\mathbf{q}_{222}|=q^*$. The sum in Eq. (18), which runs over vectors $\mathbf{q}_1$, $\mathbf{q}_2$, and $\mathbf{q}_3$ in the first shell, $\mathbf{q}$ being any fixed vector of this shell, contains 27 terms which, however, are not all equal because not all quadrilaterals formed by $\mathbf{q}$, $\mathbf{q}_1$, $\mathbf{q}_2$, and $\mathbf{q}_3$ have the same shape. When Eqs. (15)–(17) are solved for the η_2's and inserted into Eq. (18), an equation for $\eta_1(q^*)$ results that either has two or zero solutions, depending on the values of the second- to fourth-order direct correlation functions and on the sign of ρ_2. As realistic models will have fcc solutions corresponding to stable or metastable solid states below ρ_c, we expect the fcc branch to bifurcate into the negative direction, i.e., to find solutions for negative ρ_2.

In order to estimate the stability of the fcc and bcc solutions, we calculate the free-energy for both states to leading order in the parameter ϵ. We define the free- energy density difference $\Delta f=(F[\{\rho(\mathbf{r})\}]-F[\rho_b])/V$ between the liquid and the solid. It is straighforward to derive the expansion

$$\beta\Delta f=\sum_{n=2}^{\infty}\sum_{\mathbf{q}_1}\cdots\sum_{\mathbf{q}_n}\delta(\mathbf{q}_1+\cdots+\mathbf{q}_n)\,\eta(q_1)\cdots\eta(q_n)\times\left(\frac{(-1)^n}{n(n-1)}\rho_b-\frac{\rho_b^n}{n!}\tilde{c}^{(n)}(\rho_b,\mathbf{q}_1,\ldots,\mathbf{q}_{n-1})\right). \quad (19)$$

This expression actually is the Landau expansion of the general mean field free energy Eq. (1) up to arbitrary order, including secondary and higher order parameters $\eta(q\neq q^*)$. Inserting Eqs. (7) and (8), one obtains for the bcc solution

$$\beta\Delta f_{\mathrm{bcc}}=-2\epsilon^3\eta_1^2(q^*)\rho_c[1+\rho_c^2\tilde{c}^{(3)}(q^*,0)], \quad (20)$$

where $(\partial/\partial\rho)\tilde{c}^{(2)}(\rho,q)=\tilde{c}^{(3)}(\rho,q,0)$ has been used. In the fcc case no terms of order ϵ^3 occur and Eqs. (15)–(18) have to be applied to simplify the $O(\epsilon^4)$ term, which after some algebra results in the surprisingly similar expression

$$\beta\Delta f_{\mathrm{fcc}}=\mp 2\epsilon^4\eta_1^2(q^*)\rho_c[1+\rho_c^2\tilde{c}^{(3)}(q^*,0)]. \quad (21)$$

III. GLOBAL BEHAVIOR OF THE SOLUTIONS: UNSTABLE AND STABLE BRANCHES

After we have determined in the preceding section the asymptotic solutions close to the spinodal, their significance will become clearer if we look at the global behavior of the different solution branches. To this end we construct in this section generic bifurcation diagrams for the freezing to fcc and bcc solids which follow from the results of the preceding section together with some plausible assumptions on the existence of solid solutions of the Euler Lagrange equation at lower densities. First we observe that the liquid state is locally stable for $\rho_b<\rho_c$ but unstable for $\rho_b>\rho_c$. At unstable solutions there are directions in the $\eta(q)$ space that lower the free energy, i.e., these solutions are saddle points of $\Delta f[\{\eta(q)\}]$. Since the solutions obtained by the bifurcation analysis are those closest to the liquid in the vicinity of ρ_c, they must be unstable for $\rho_b<\rho_c$. On the other hand, a realistic theory that predicts a first-order freezing transition will also have stable solutions below the spinodal, with a larger degree of order. It is natural to assume that these are connected to the unstable branch at a point where higher derivatives of Δf vanish, which leads to the situation depicted in Fig. 1.

A negative value of $\eta(q^*)$ gives a lattice with maxima of $\rho(\mathbf{r})$ at the interstitials of the original lattice, i.e., the points that have maximal and equal distances from the surrounding lattice sites. For fcc the lattice formed by the interstitials is just the original lattice shifted by half the cube size along, e.g., the (100) direction. Therefore the fcc bifurcation diagram is symmetric with respect to $\eta(q^*)\leftrightarrow-\eta(q^*)$: for any solution with positive $\eta(q^*)$ an equivalent solution exists with the opposite sign of $\eta(q^*)$ [and of $\eta(q)$ with q in higher ''odd'' shells], which represents the same structure shifted in real space. On the other hand, the interstitials of the bcc lattice form a more complicated cubic lattice with a basis that is not equivalent to the bcc lattice, which explains the absence of the corresponding symmetry in Fig. 1(a). As the bcc branch for $\rho_b<\rho_c$ (i.e., $\epsilon<0$) should be connected to locally stable bcc solutions with positive $\eta(q^*)$, one expects

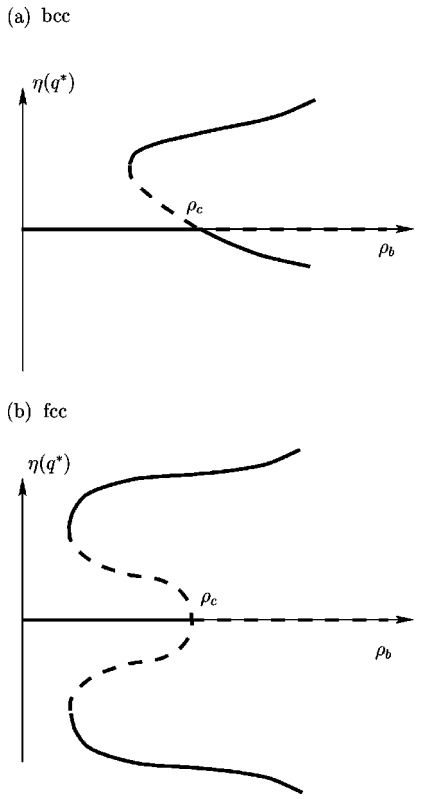

FIG. 1. Schematic bifurcation diagrams for (a) the bcc and (b) the fcc solid. The first Fourier coefficient $\eta(q^*)$ of the solidlike solutions of the Euler Lagrange equation is shown as a function of the bulk density ρ_b. Solid and dashed lines correspond to local minima and saddle points of the free energy, respectively. The slope of the unstable solid branch at the spinodal density ρ_c is finite for bcc and infinite for fcc.

$\eta_{1,\mathrm{bcc}}(q^*)<0$. Moreover the free-energy difference Δf to the liquid should be positive for the unstable branch. Both requirements are fulfilled when $1+\rho_c^2\tilde{c}^{(3)}(q^*,0)>0$ and $1+\rho_c^2\tilde{c}^{(3)}(\mathbf{q}_1,\mathbf{q}_2)>0$ for $q_1=q_2=|\mathbf{q}_1+\mathbf{q}_2|=q^*$ [see Eqs. (14) and (20)], which we expect to be generally valid in realistic theories of freezing.

The vanishing of ρ_1 for the fcc solutions, induced by the impossibility to form equilateral triangles from the vectors of the first shell in reciprocal space, leads to different power-law behaviors of Δf for the unstable branches near the spinodal: due to $\epsilon_{\mathrm{bcc}}\sim\rho_b-\rho_c$ and $\epsilon_{\mathrm{fcc}}\sim|\rho_b-\rho_c|^{1/2}$ one has $\Delta f_{\mathrm{bcc}}\sim(\rho_c-\rho_b)^3$ and $\Delta f_{\mathrm{fcc}}\sim(\rho_c-\rho_b)^2$ so that $0<\Delta f_{\mathrm{bcc}}<\Delta f_{\mathrm{fcc}}$ if comparison is made at the same bulk density (not at the same value of the order parameter as was implicitly done in Ref. [1]). Thus general symmetry-based arguments predict a lower free energy along the unstable branch of the bcc solid compared to the fcc solid. However, no general conclusion is possible concerning the relative depths of the bcc and fcc minima represented by the upper branches in Fig. 1. These depend on the details of the full functional and cannot be determined from a local analysis at the bifurcation point. Results of density-functional theories for hard spheres indicate, in agreement with simulation results, that the solid density at liquid-solid coexistence is strongly peaked and cannot be described by one or a few Fourier components in Eq. (5) [10]. But, even if the stable branches were close

enough to the liquid at $\rho_b \simeq \rho_c$ so that a truncation of Eq. (19) after the fourth term was a good approximation, a general statement would still be impossible due to the dependence on $\tilde{c}^{(4)}$. The more universal second- and third-order terms alone obviously are not sufficient to produce stable solutions at all. Therefore we repudiate Alexander and McTague's conclusion that bcc should be favored (as the stable solid phase) when the first-order character of the transition is not too pronounced.

The above result concerning the height of the free energy barrier in order parameter space between the liquid and the stable solid branches may be relevant for the nucleation of the solid phase, although we have assumed translational invariance of $\rho(\mathbf{r})$ from the beginning, whereas nucleation usually takes place via spatially inhomogeneous nuclei. Still computer simulations [6,7] as well as density-functional calculations [8] provide evidence for the occurrence of local bcc stucture within these nuclei in systems with stable fcc phases. An earlier application of symmetry arguments to nucleation was given by Klein and Leyvraz [11], who, however, used a concrete example for the functional and did not discuss fcc solutions because they only took into account the first two bifurcation equations. Their conclusion is that the critical nucleus must have bcc symmetry near the spinodal.

Along the same lines we can discuss the stability of an icosahedral quasicrystal for which the first shell in reciprocal space is formed by the edges of a regular icosahedron. Here the sum in Eq. (10) has four terms if $q_1 = q_2 = q = q^*$, as for the bcc case. Therefore the amplitude of the bifurcating solutions is again given by Eq. (14). However, the corresponding free energy is

$$\beta \Delta f_{\mathrm{ico}} = -5\epsilon^3 \eta_1^2(q^*)\rho_c[1+\rho_c^2 \tilde{c}^{(3)}(q^*,0)]. \tag{22}$$

Hence below the spinodal (i.e., for $\epsilon < 0$) the free energy of the unstable branch is higher for the icosahedral structure than for bcc by a factor 5/2.

By the same methods we find that for the hypothetical triangular lattice mentioned above the amplitude of the bifurcating solutions is twice that given by Eq. (14) and the corresponding free-energy difference to the liquid is twice as large as that of the bcc structure.

IV. A SIMPLE EXAMPLE

In this section we consider a specific example for the density functional to illustrate and corroborate the general findings of the preceding sections. Specifically, we employ the second virial approximation for the excess free energy

$$F_{\mathrm{ex}}[\{\rho(\mathbf{r})\}] = -\frac{1}{2}\int d^3r d^3r' \rho(\mathbf{r})\rho(\mathbf{r}') f(|\mathbf{r}-\mathbf{r}'|), \tag{23}$$

where $f = \exp(-\beta w) - 1$ is the Mayer function for the interaction potential w. We consider a hard sphere potential for particles of diameter σ so that $f(r) = c^{(2)}(r) = -\Theta(r-\sigma)$. This approximation has many merits in the field of liquid crystals but it is reliable only for low bulk densities. At densities near the freezing transition it does not yield quantitatively reasonable results, but still captures the essential qualitative features. A short discussion of more sophisticated density functionals will be given in the next section.

Instead of a full minimization with respect to an arbitrary solidlike $\rho(\mathbf{r})$, we follow the usual strategy to make a trial parametrization of the inhomogeneous density and to minimize only with respect to a small number of parameters. First we examine the commonly applied Gaussian approximation

$$\rho(\mathbf{r}) = \frac{\rho_b}{\rho_s}\left(\frac{\alpha}{\pi}\right)^{3/2} \sum_{\mathbf{R}} e^{-\alpha(\mathbf{r}-\mathbf{R})^2}, \tag{24}$$

where the parameter α measures the width of the density peaks that are located at the lattice sites $\mathbf{R}$. The density of the lattice sites ρ_s (and thus the magnitude of the lattice vectors) is treated as an additional minimization parameter and not fixed by the bulk density ρ_b. Thus solutions with more or less than one particle per site are included. The corresponding Fourier coefficients are

$$\eta(q) = e^{-q^2/4\alpha}, \tag{25}$$

where the absolute values of the wave vectors in the first shell for fcc and bcc lattices are

$$q_1^{\mathrm{fcc}} = 2\pi\sqrt{3}\left(\frac{\rho_s}{4}\right)^{1/3}, \quad q_1^{\mathrm{bcc}} = 2\pi\sqrt{2}\left(\frac{\rho_s}{2}\right)^{1/3}. \tag{26}$$

The excess free energy is calculated from

$$\beta F_{ex}/V = -\frac{1}{2}\rho_b^2\left(\tilde{f}(0) + \sum_q \eta(q)^2 \tilde{f}(q)\right) \tag{27}$$

with the Fourier transformed Mayer function

$$\tilde{f}(q) = -4\pi\sigma^3 \frac{\sin q\sigma - q\sigma\cos q\sigma}{(q\sigma)^3} \tag{28}$$

using q values of the lowest 10 to 20 shells. For the ideal contribution to the free energy, one has the expansion

$$\beta F_{\mathrm{id}}/V = \rho_b(\ln \rho_b \lambda^3 - 1) + \rho_b \sum_{n=2}^{\infty} \frac{(-1)^n}{n(n-1)} \times \sum_{\mathbf{q}_1} \cdots \sum_{\mathbf{q}_n} \delta(\mathbf{q}_1 + \cdots + \mathbf{q}_n)\,\eta(q_1)\cdots\eta(q_n). \tag{29}$$

The sums over $\mathbf{q}_i$ can be replaced by sums over shells when appropriate coefficients $a_{q_1 \cdots q_n}$ are added that take into account the number of possibilities to add vectors from shells $q_1, \ldots, q_n$ to zero. These coefficients have been calculated (for $n \leq 10$) by a short MATHEMATICA program. While Eq. (29) is very convenient for small values of α, when $\eta(q)$ decreases quickly with increasing q, the series does not converge for larger q. [The convergence radius is 1/8 if $\eta(q_1)$ is assumed to be the only nonzero Fourier coefficient.] Therefore we used Eq. (29) only for those (α, ρ_s) for which $\eta(q_1) \leq 0.09$, while for larger α the three-dimensional integral

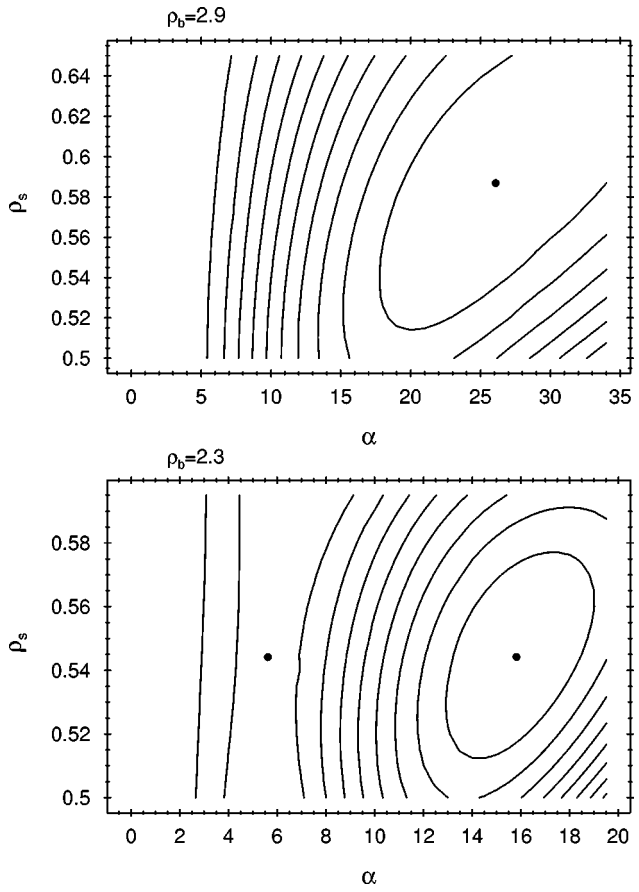

FIG. 2. Contour plots of the free energy of a fcc structure within the Gaussian density approximation as a function of the width parameter α and the lattice site density ρ_s for bulk densities above and below the bifurcation density $\rho_c = 2.7705$. The black dots denote stationary points.

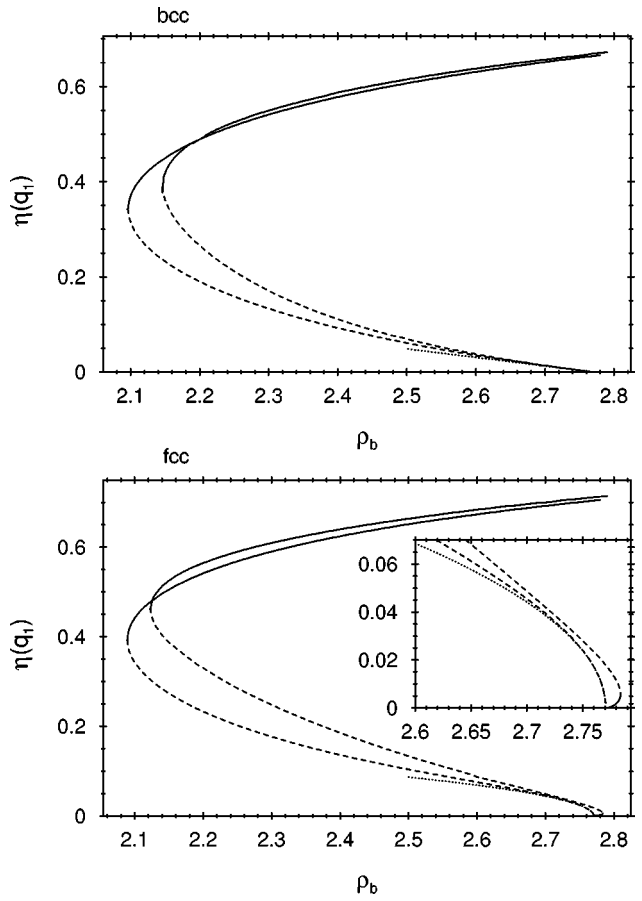

FIG. 3. Bifurcation diagrams for bcc and fcc solutions of the stationarity equation. The first Fourier coefficient is shown as a function of the bulk density. The upper curves are calculated with the Gaussian ansatz Eq. (24), the lower curves with the cumulant ansatz Eq. (31). Solid lines correspond to local minima, dashed lines to saddle points. The dotted lines represent the asymptotic behavior near the bifurcation point, which is linear for bcc and square-root-like for fcc.

$$\beta F_{\mathrm{id}}/V = \frac{1}{V_c}\int_{V_c} d^3r\,\rho(\mathbf{r})[\ln \rho(\mathbf{r})\lambda^3 - 1] \tag{30}$$

over the unit cell V_c was calculated numerically using a standard routine.

The bifurcation density of this model, obtained from Eq. (13) with $\tilde{c}^{(2)}(\rho_c, q) = \tilde{f}(q)$, is $\rho_c = 2.770$ and the critical wave number $q^* = 5.763$; here and in the following σ is used as the unit of length. The site densities at the bifurcation point are $\rho_s^{\mathrm{fcc}} = 0.5941$ and $\rho_s^{\mathrm{bcc}} = 0.5458$. The enormous difference between ρ_s and ρ_c as well as the fact that ρ_c is much larger than the density of close packing of hard spheres are due to the crudeness of the density-functional approximation.

Contour plots of $F(\rho_s, \alpha)$ at bulk densities above and below ρ_c are shown in Fig. 2. For $\rho_b > \rho_c$, F decreases from the constant value $F(\rho_s, 0)$ for the liquid with increasing α and exhibits a minimum corresponding to a quite strongly peaked structure. The ratio of the decay length $1/\sqrt{\alpha}$ to the nearest-neighbor distance is 0.147 at the minimum for the case shown in Fig. 2(a). On the other hand, the liquid is locally stable for $\rho_b < \rho_c$ and a saddle point occurs at an intermediate value of α in addition to the solid minimum. It is this saddle point that is accessible by the bifurcation analysis of Sec. II. We tracked the positions of the saddle point and the minimum as a function of the bulk density by numerical solution of $\partial F/\partial \rho_s = \partial F/\partial \alpha = 0$ (see Fig. 3). Expressions for the partial derivatives can easily be derived from Eqs. (27), (29), and (30). As expected, both stationary points approach each other for decreasing ρ_b and merge at a certain threshold density below which no solid solution exists. However, in the immediate vicinity of ρ_c the fcc solutions show a peculiar behavior [see the inset in Fig. 3(b)]: attached to the unstable branch one finds a short additional branch of stable solutions which approaches the bifurcation point with a power law $\sim(\rho_b - \rho_c)^{3/2}$. This artifact is a consequence of the restricted parameter space that enforces a fixed relationship between the first and second shell coefficients [Eq. (25)], e.g., $\eta(q_{200}) = \eta(q_{111})^{4/3}$, which is not compatible with the behavior of the exact solution [see Eq. (15)].

These problems are avoided with a more general ''cumulant'' ansatz for the density

$$\rho(\mathbf{r}) = C \exp\left(-\sum_{j=1}^{n} \alpha_j \sum_{\mathbf{q}\in S_j} e^{i\mathbf{q}\cdot\mathbf{r}} \right), \tag{31}$$

where j runs over the first n shells S_j. The constant $C = C[\{\alpha_j\}]$ is fixed by the normalization $\int d^3r\,\rho(\mathbf{r}) = \rho_b V$.

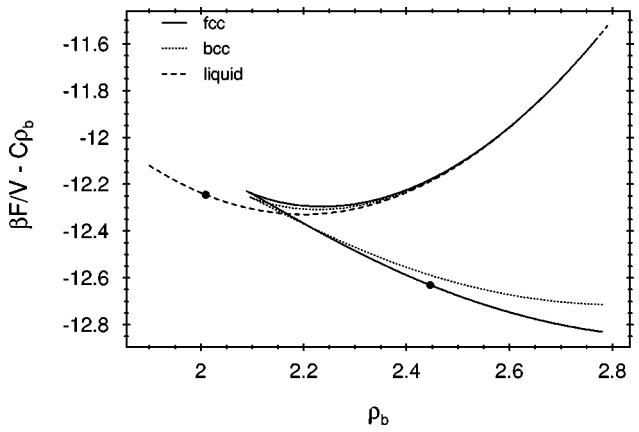

FIG. 4. Free energy along the unstable (upper parts) and stable (lower parts) solution branches for fcc and bcc structures obtained with the cumulant ansatz. Also shown is the free energy of the liquid. To make the differences more clearly visible, a linear function of the bulk density has been substracted. This does not prevent the possibility to determine phase coexistence by the double tangent construction from these curves which yields the densities of the coexisting liquid and fcc solid marked by black dots.

This ansatz allows independent variations of the first n Fourier coefficients while for large values of the α_j it approximately reproduces the Gaussian behavior near the lattice points. Actually for the stable branches it yields lower free energies than the Gaussian ansatz, indicating that it is closer to the exact solution. We set $n=4$ which includes all shells that can be reached by a sum of two first shell vectors, i.e., those for which $\eta_2(q)\neq 0$ according to the bifurcation analysis. The Fourier coefficients $\eta(q)$ (and the constant C) are determined by three-dimensional fast Fourier transformation with 16 points in each dimension. The excess free energy is then again obtained from Eq. (27) while the ideal free energy is

$$\beta F_{\mathrm{id}}/V=\rho_b\left[\ln C-1+\sum_{j=1}^{n} N_j\alpha_j\eta(q_j)\right], \qquad (32)$$

N_j being the number of vectors in shell S_j. Figure 3 shows that with this ansatz, $\eta(q_1)$ of the saddle point branch approaches the liquid axis with an infinite slope and with the amplitude predicted by Eqs. (15)–(18).

Results for the free energy along the various solution branches are presented in Fig. 4. In order to make the differences more visible, the function $K\rho_b$ with an appropriately chosen value of K was substracted. The unstable bcc branch indeed lies below the unstable fcc branch, as predicted by the general analysis. However, this relationship is reversed for the *stable* branches for densities $\rho_b>2.2$. Phase coexistence can be determined from Fig. 4 by the double tangent construction, which yields a liquid-fcc transition while the liquid-bcc coexistence is only metastable. Already this simple example shows the mechanism that can favor the fcc structure as the stable phase in spite of the exceptional role played by the bcc structure in the vicinity of the bifurcation point.

V. CONCLUSIONS

In summary, we have shown that the liquid state becomes unstable to solid fluctuations of different symmetries at the same spinodal density ρ_c. The symmetry differences between fcc and bcc structures manifest themselves in different exponents for the density dependence of the order parameter and the free energy below ρ_c along the bifurcating branches. But, since these branches correspond to unstable solutions, the bcc structure generically has a lower maximum in the free energy than fcc, not a lower minimum as implied by Alexander and McTague, whereas a small order parameter expansion cannot access the relative stability of the stable branches. For Onsager's second-virial density-functional theory of the isotropic-nematic transition, it has been shown that even if the bifurcation analysis is carried through to very high order, it only captures the unstable branch up to the inflection point [12].

The relation of our results to the observation of bcc order in nucleation phenomena is not straightforward because only bulk fluctuations were considered. A rigorous treatment of spatially inhomogeneous nucleating clusters is probably not feasible within bifurcation analysis because the structure of the core of the nucleus will be close to the stable bulk branch. However, near the spinodal the nucleus will exhibit reduced crystalline order across a *broad* interface to the metastable liquid. Therefore its free energy of formation may be approximated by an integral over the bulk free energy corresponding to the local degree of order at a given radial distance. This integral will be dominated by the contributions of structures near the unstable branch. This reasoning would predict a preference for bcc order in the interface of the cluster, in accordance with the simulation results [6,7].

We add a final remark concerning the relevance of our results to the cases of more realistic (compared to the second-virial approximation of Sec. IV) density-functional theories for hard spheres. They are often explicitly constructed in a way that reproduces the Percus-Yevick approximation to the liquid direct correlation function. In this case Eq. (13) has no solution for packing fractions $\eta<1$, which means that there is no liquid-solid spinodal. However, since the Percus-Yevick result presumably is not a very accurate description of the structure of the strongly ''supercompressed'' liquid, it is not clear at the present stage what the corresponding behavior of the *exact* density functional would be.

ACKNOWLEDGMENTS

This work is part of the research program of the Stichting voor Fundamenteel Onderzoek der Materie (Foundation for Fundamental Research on Matter) and is made possible by financial support from the Nederlandse Organisatie voor Wetenschappelijk Onderzoek (Netherlands Organization for the Advancement of Research). B.G. acknowledges the financial support of the EU through the Marie Curie TMR Fellowship Programme.

[1] S. Alexander and J. McTague, Phys. Rev. Lett. **41**, 702 (1978).
[2] L. Landau, Zh. Eksp. Teor. Fiz. **7**, 19 627 (1937) [English translation in *The Collected Papers of L.D. Landau*, edited by D. ter Haar (Gordon and Breach–Pergamon, New York, 1965), p. 193].
[3] J.-C. Tolédano and P. Tolédano, *The Landau Theory of Phase Transitions* (World Scientific, Singapore, 1987).
[4] Y. Singh, Phys. Rep. **207**, 351 (1991).
[5] H. Löwen, Phys. Rep. **237**, 249 (1994).
[6] P. ten Wolde, M. Ruiz-Montero, and D. Frenkel, Phys. Rev. Lett. **75**, 2714 (1995).
[7] P. ten Wolde, M. J. Ruiz-Montero, and D. Frenkel, J. Chem. Phys. **104**, 9932 (1996).
[8] Y. C. Shen and D. W. Oxtoby, Phys. Rev. Lett. **77**, 3585 (1996).
[9] D. Shechtman, I. Blech, D. Gratias, and J. Cahn, Phys. Rev. Lett. **53**, 1951 (1984).
[10] B. Laird, J. McCoy, and A. Haymet, J. Chem. Phys. **88**, 3900 (1988).
[11] W. Klein and F. Leyvraz, Phys. Rev. Lett. **57**, 2845 (1986).
[12] R. Kayser and H. Raveché, Phys. Rev. A **17**, 2067 (1978).